Electronic Supplementary Material (ESI) for Chemical Science.
This journal is © The Royal Society of Chemistry 2018

ELECTRONIC SUPPLEMENTARY INFORMATION

Luminescent mesoporous nanorods as photocatalytic enzyme-like peroxidase surrogates

M. Carmen Ortega-Liebana,[a,b] Jose L. Hueso,*[a,b] Rodrigo Fernandez-Pacheco,[c] Silvia Irusta[a,b] and Jesus Santamaria*[a,b]

[a]Institute of Nanoscience of Aragon (INA) and Department of Chemical Engineering and Environmental Technology, University of Zaragoza, 50018 Zaragoza, Spain.
[b]Networking Research Center on Bioengineering, Biomaterials and Nanomedicine (CIBER-BBN), 28029 Madrid, Spain.
[c]Advanced Microscopy Laboratory (LMA) and Institute of Nanoscience of Aragon (INA), University of Zaragoza, 50018 Zaragoza, Spain.

Summary of information provided:

Table S1. Summary of the different thermal treatments carried with the mesoporous nanorods.
Table S2. Specific surface values, pore sizes and pore volumes for untreated and treated mesoporous nanorods.
Table S3. Summary of the XPS analysis parameters for the luminescent mesoporous nanorods.
Table S4. Summary of the current state-of-the-art nanomaterials with peroxidase-mimicking activity.
Figure S1. Small-angles X-ray diffraction patterns corresponding to the LMS@C, LMS@Si@C and LMS@Si samples.
Figure S2. Representative TEM and STEM images after the different flash-thermal treatments
Figure S3. Control experiments carried out to demonstrate the presence of carbogenic dots after the digestion of the silica structure under strong basic conditions. Analysis of the dialyzed samples by TEM and Fluorescence spectroscopy.
Figure S4. Control experiment to confirm the association of the PL response in the LMS@Si sample and the presence of silica-based emitting centers. Evolution of the PL spectra before and after digestion in strong basic conditions and subsequent dialysis
Figure S5. Influence of the LED irradiation time on the peroxidase-mimicking performance of the LMS catalysts towards the oxidation of TMB in the presence of H_2O_2.
Figure S6. Control experiments in the absence of light or LMS catalysts.
Figure S7. Control experiment in the absence of hydrogen peroxide in the peroxidase-like activity of the LMS@Si@C.
Figure S8. Investigation of the effect of illuminating with different LED wavelengths on the photocatalytic activity of the different catalysts.
Figure S9. Digital images of the experimental setup and schematic display of the experimental setup for peroxidase enzymatic assays using TMB performed in MW24 cell culture plates.
Fig. S10. Detection of hydroxyl radicals ($^{\bullet}OH$) generated from H_2O_2 and schematic illustration of the colorimetric assay performed to identify the presence of hydroxyl radicals using disodium terephthalate (NaTA).
Figure S11. Influence of the initial concentration of the LMS@Si@C sample on the final performance as peroxidase-mimicking surrogate.
Figure S12. Influence of the reaction temperature on the peroxidase-like activity of the LMS@Si@C catalyst in comparison with the photo-enhanced response observed after 5 min irradiation with a blue LED at 405 nm.
Figure S13. Reusability of the peroxidase-like catalyst after 3 consecutive cycles.
Figure S14. Use of the LMS@Si@C in the indirect and selective detection of glucose.

Electronic Supplementary Information References

Table S1. Summary of the different thermal treatments carried out on the mesoporous nanorods and the corresponding photoluminescent responses.

Sample	Heating treatment	Reaction Conditions	Photoluminescence spectrum	Remarks
Mesoporous Nanorods	No thermal activation		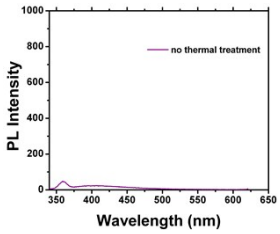	No PL emission SiO_2 network
FH[a]. N_2 flow **(1)**	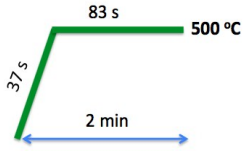	Flowing N_2 as carrier gas	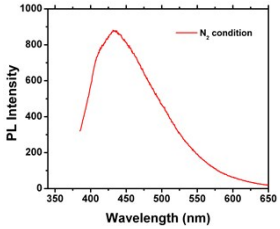	PL emission maximum centered at 434 nm **Preferential generation of C-dots** **LMS@C**
(1) + Calcination in air	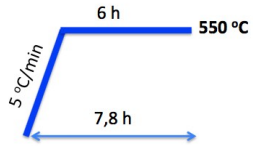	Air	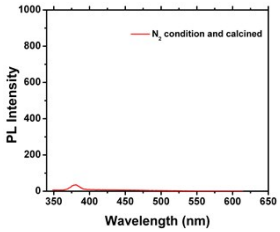	No PL emission SiO_2
FH. N_2 static **(2)**	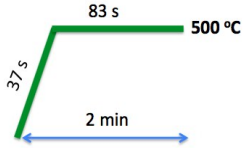	Reactor initially fed with N_2 (no continuous flow of carrier gas)	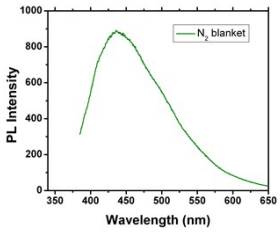	Emission max 432 nm **C-dots, oxygen-deficient silica centers, Si-C-O**
(2) + Calcination in air	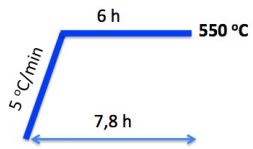	Air	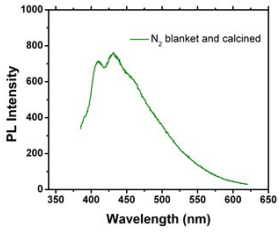	Emission max 426 nm **Oxygen-deficient silica centers, Si-C-O domains**

FH. Static Air **(3)**		Reactor not fed with any flowing carrier gas (static air)	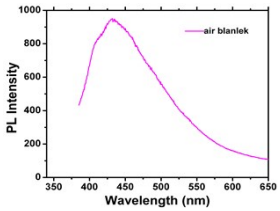	Emission max 437 nm **C-dots, oxygen-deficient centers, Si-C-O domains.** **LMS@Si@C**
(3) + Calcination in air		Air	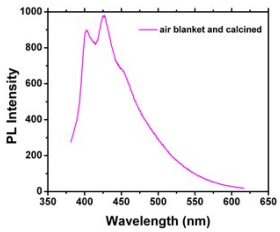	Emission max 431 nm **Oxygen-deficient silica centers, Si-C-O domains** **LMS@Si**
CH[b] **(1)**	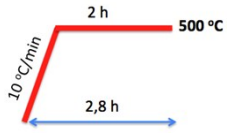	Flowing N_2	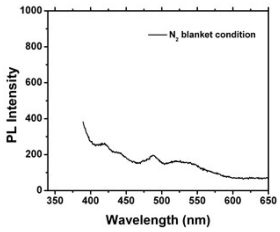	No emission SiO_2
CH **(2)**	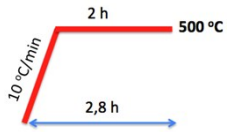	Reactor not fed with any flowing carrier gas (static air)	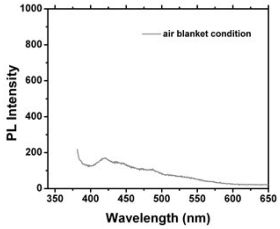	No emission SiO_2

[a] **FH:** flash-thermal heating treatment carried out in a fluidized-bed reactor;
[b] **CH:** conventional heating treatment carried out in a tubular reactor.

Table S2. Specific surface values, pore sizes and pore volumes calculated from the N_2 adsorption–desorption isotherms for untreated and treated mesoporous nanorods.

Sample	**S_{BET} [m^2g^{-1}]**	**Pore size [nm]**	**Total pore Volume [cm^3g^{-1}]**
MS	456.8	10.3	1.2
LMS@C	454.8	9.1	1.1
LMS@Si@C	481.3	9.3	1.2
LMS@Si	552.8	8.5	1.2

Table S3. Surface chemistry analysis of the luminescent mesoporous nanorods. Fitted X-ray photoemission assignations of the C1s, O1s and Si 2p region in the LMS@C, LMS@Si@C and LMS@Si samples, respectively.

Sample	C 1s	O 1s	Si 2p
	Binding energy, eV (At %)	Binding energy, eV (At %)	Binding energy, eV (At %)
LMS@C	284.2 C-C/C=C/C-H (9.14)	532.3 SiO_2 (49.36)	102.0 Si-CH_x (9.74)
	285.3 C-O (6.2)		102.8 Si-O (24.52)
	287.9 C=O (1.04)		
LMS@Si@C	284.2 C-C/C=C/C-H (1.72)	530.4 C=O(58.82)	101.9 Si-CH_x (9.27)
	285.6 C-O (1.21)	532.2 SiO_2 (2.71)	101.1 Si-Si (26.23)
	287.9 C=O (0.04)		
LMS@Si	284.2 C-C/C=C/C-H (2.11)	530.6 (36.36)	101.9 Si-CH_x (20.86)
	282.7 C-Si (0.51)	531.7 SiO_2 (20.39)	101.1 Si-Si (6.15)
	285.9 C-O (1.84)		103.3 Si-O (11.79)

Table S4. Summary of the current state-of-the-art nanomaterials claiming a peroxidase-mimicking activity reported in the literature. Overview of multiple experimental conditions and kinetics parameters.

Catalyst[REF]	Substrate	K_m [mM]	V_{max} .10^{-8} [M s^{-1}]	K_{cat} (s^{-1}) or Time	pH	Temp (ºC)	Detection of glucose	
							Linear range	DL
[a]C-Dots[1]	TMB H_2O_2	0.039 ± 0.001 26.77 ± 2.94	3.61 ± 0.012 30.61 ± 0.38	10 min	4	35	0.001-0.50 mM	0.4 µM
[b]Si-Dots[2]	TMB H_2O_2	1.502 0.065	14.72 5.62	30 min	4	40	0.17-200 µM	0.05 µM
Pt/[c]CDs[3]	TMB H_2O_2			5 min	4-6			
[h]GFH[4]	TMB H_2O_2			400 sec	7	RT		
[d]GO-Fe_2O_3[5]	TMB H_2O_2	0.228 305	5.38 10.1	60 min	3.6	25		
[e]GO-COOH[6]	TMB H_2O_2		0.0237 ± 0.001 3.99 ± 0.67	600 sec	5	35	1-20 µM	1 µM
[d]GO-Au[f]NCs[7]	TMB H_2O_2	0.16 142.39		196.8 607.6 and 600 sec	7	37		
Hemin-[i]SWCNT[8]	H_2O_2	0.08 ± 0.003	4.79 ± 0.21	15 min	4.3	37	0.5-200 µM	0.2 µM
[d]GO-Fe_3O_4[9]	TMB H_2O_2	0.43 0.71	13.08 5.31	15 min	4	40	2-200 µM	0.74 µM
Fe_3O_4@Carbon[10]	TMB H_2O_2	0.072 0.38	17.99 73.99	10 min	3	45		

Fe_3O_4 [r]NSs /[e]rGO[11]	H_2O_2	0.25		15 min	4	RT		
[j]NDAus[12]	OPD H_2O_2	48.7 ± 0.2 208.7 ± 14.7	5.9 ± 0.3* 1.8 ± 0.2*	290.4± 21.2* 377.6± 22.9*	7.2	RT		
				300 sec				
[f]CNDs[13]				20 min	4	RT	1-5 μM	0.5 μM
Cu-Ag/[e]rGO[14]	TMB H_2O_2	0.6340 8.6245	4.2553 7.0175	30 min	3.8	35	1-30 μM	3.85 μM
Magnetosome[15]	TMB H_2O_2	0.90 17.65	44.5 11.9	360 s	4	28, visible-light		
MoS_2/[d]GO[16]	TMB H_2O_2	0.10± 0.23 0.20 ± 0.05	33.40 ± 3.34 19.70 ± 2.26	10 min	4	25, visible-light	1-50 μM	86 nM
EDTA[17]	GNRs H_2O_2			6 min		UV Light		
[m]BSA-Au [f]NCs[18]	TMB Without H_2O_2	0.08	9.59	10 min	3	Visible light		
[g]g-C_3N_4[19]	TMB H_2O_2			30 min	3	60	5-100 μM	1 μM
[q]CS-AgI[20]	TMB Without H_2O_2	0.0228	16.9	10 min	3-7	Visible light		
[p]CdS[21]	TMB H_2O_2	0.0054 6.54		100sec	4	40		
[p]CdS[22]	TMB H_2O_2	0.0095 3.62	3.57 5.6	150 sec	4	40		
[o]SiNWAs[23]	[s]OPD H_2O_2			60 min		37		
LMS@Si@C **This work[#]**	TMB H_2O_2	0.0525 ± 0.00734 0.02995 ± 0.00235	0.1488 ± 0.00412 0.3112 ± 0.0509	5 min	5-7	Blue-LED irradiation	10-130 μM	0.5 μM

* for mg^{-2}

[#] Average for three replicates

[a)]C: carbon; [b)]Si: silicon; [c)]CDs: carbon dots; [d)]GO: graphene oxide; [e)]rGO: reduce graphene oxide; [f)]CNDs: carbon nitride dots; [g)]g-C_3O_4: graphite-like carbon nitride; [h)]GFH: graphene-hemin composite; [i)]SWCNT: single-walled carbon nanotubes; [j]NDAus: nanodiamond gold nanocomposites; [k)]GFH: graphene-hemi composite.; [m)]BSA: bovine serum albumin; [n)]AuNCs: nanoclusters; [o)]SiNWAS: silicon nanowire arrays; [p)]CdS: cadmiun sulfide nanoparticles; [q)]CS: Chitosan; [r)]NSs: nanospheres; [s)]OPD: 1,2-phenylenediamine (peroxidase substrate).

ADDITIONAL FIGURES

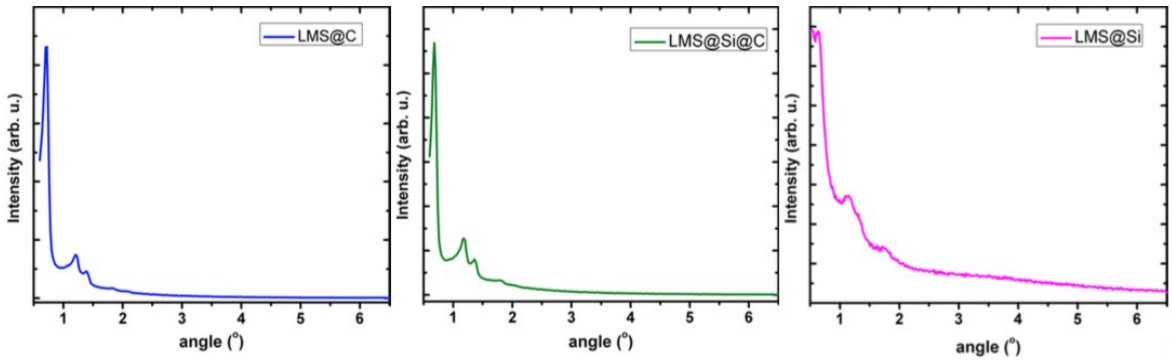

Fig. S1 Small-angle X-ray diffraction patterns corresponding to the LMS@C, LMS@Si@C and LMS@Si samples. It can be found that both samples LMS@C and LMS@Si@C show three diffraction peaks, were indexed to (100), (110), (200) which are characteristic of 2D hexagonal mesoporous silica SBA-15. The LMS@Si mesoestructures showed a peak, which was indexed as (100). This shows that the LMSs mesostructure is maintained after the flash-thermal treatments.

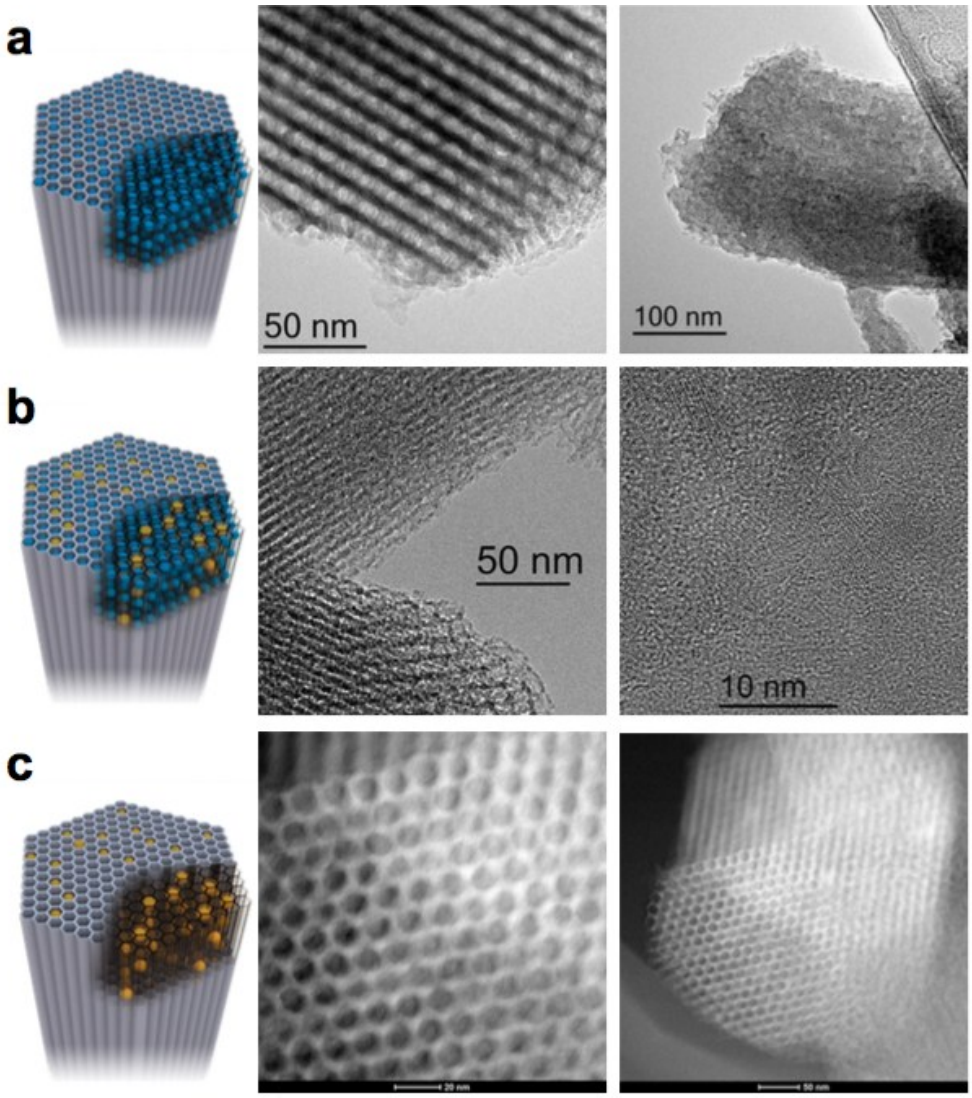

Fig. S2 Representative TEM and STEM images of the rod-shaped mesoporous nanostructures after the different flash-thermal treatments: a) LMS@C; b) LMS@Si@C and c) LMS@Si, respectively.

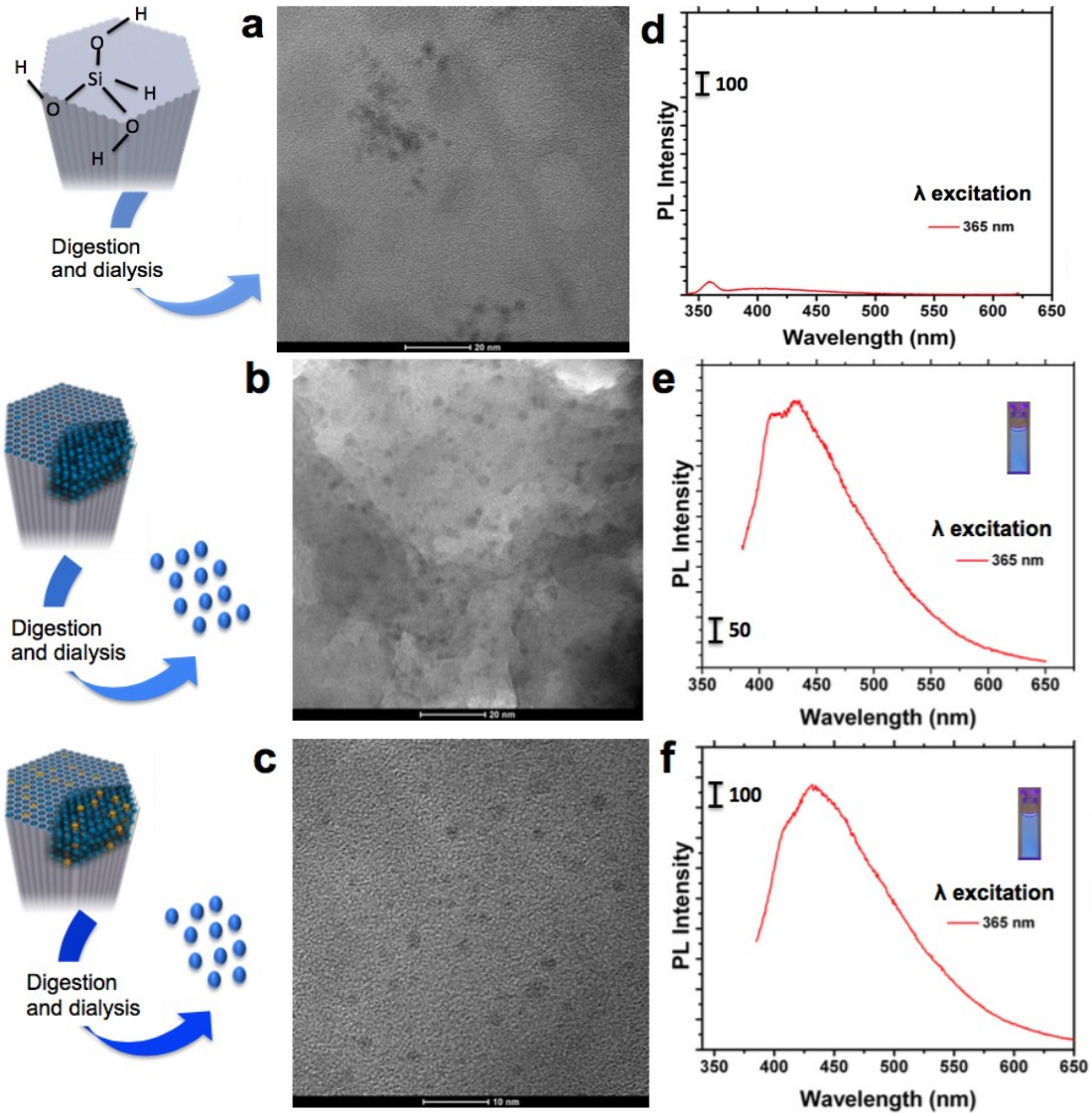

Fig. S3 Control experiments carried out to demonstrate the presence of carbogenic dots after the digestion of the silica structure under strong basic conditions. Analysis of the dialyzed samples by TEM and Fluorescence spectroscopy: a) TEM analysis of the non-treated samples after digestion and dialysis; b) TEM analysis of the LMS@C sample after digestion and dialysis where the presence of carbon dots is observed; c) TEM analysis of the LMS@Si@C sample after digestion and dialysis, again displaying the presence of carbon dots; d-f) Photoluminescence spectrum after basic digestion and dialysis of (d) the non-treated mesoporous rod; (e) the LMS@C sample (f) the LMS@Si@C sample.

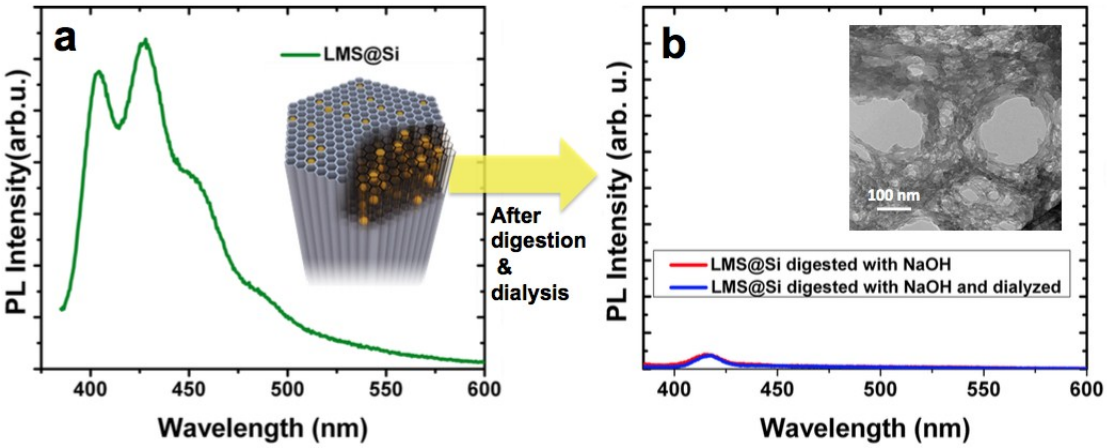

Fig. S4 Control experiment to confirm the association of the PL response in the LMS@Si sample with the presence of silica-based emitting centers. PL spectra before (a) and after (b) digestion of the silica matrix under strong basic conditions and subsequent dialysis: a) PL spectrum of the LMS@Si sample; b) PL spectrum of the same sample after digestion with NaOH and dialysis (inset: TEM image of silica remains).

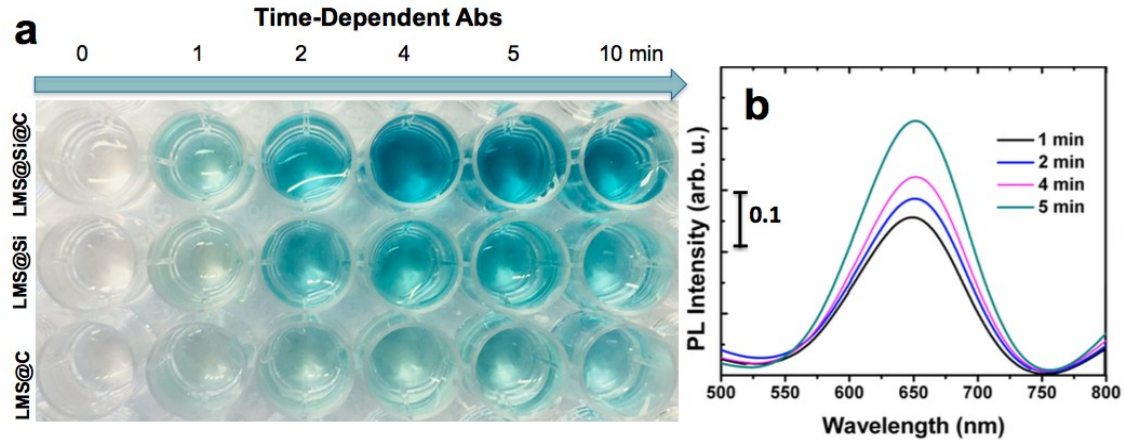

Fig. S5 Performance of the different LMS catalysts towards the oxidation of TMB in the presence of H_2O_2: a) Digital photograph showing progressive coloration due to the oxidation of TMB under a blue-emitting LED at 405 nm (up to 10 minutes). b) UV-Vis absorption spectra displaying the evolution of the TMBox upon increasing irradiation times with the blue LED. Experimental details: [H_2O_2] = 10 mM; [LMSs] = 4 µg mL^{-1}; [TMB] = 0.16 mM; pH = 7.4 in 0.2 M NaAc buffer; irradiation experiments with a blue LED (λ_{exc} = 405 nm); and reaction temperature: 19-20 °C.

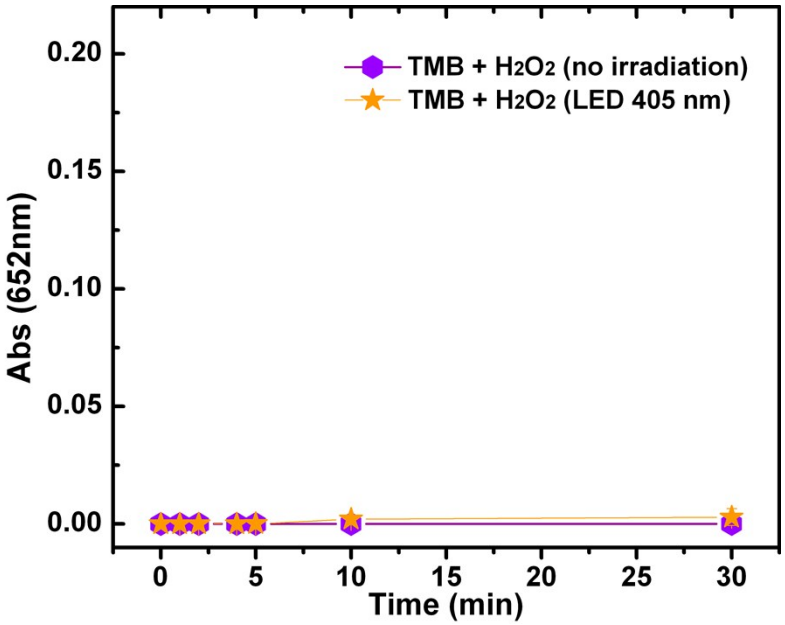

Fig. S6 Control experiments in the absence of light or LMS catalysts. Time-dependent evolution of the maximum in the absorbance of the TMB oxidized intermediate centered at 652 nm for the TMB+H_2O_2 (no irradiation, no catalyst) and TMB+H_2O_2 + LED 405 nm (no catalyst).

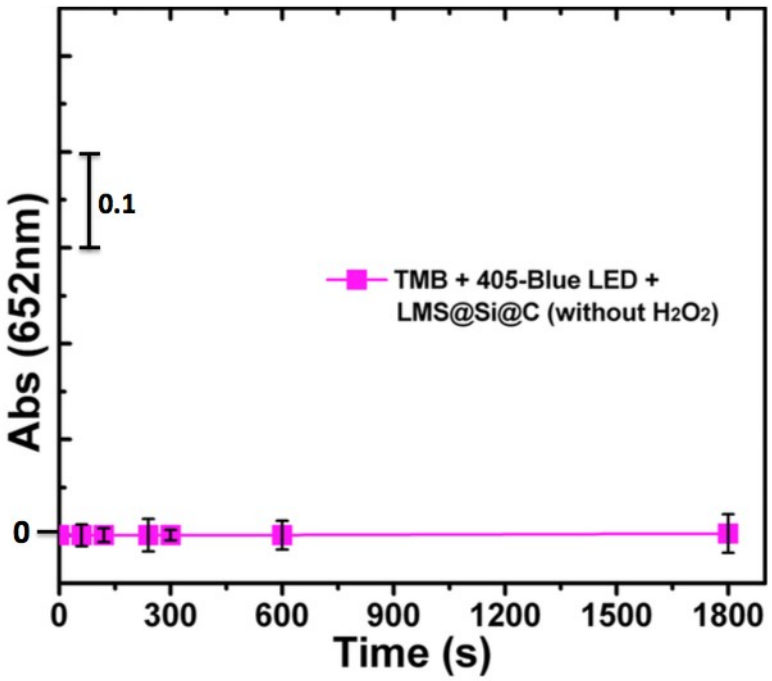

Fig. S7 Control experiment to evaluate the absence of hydrogen peroxide in the peroxidase-like activity of the LMS@Si@C enzyme-like photocatalyst. Time-dependent absorbance charge TMB at 652 nm for the LMS@Si@C after 30 min of irradiation with Blue-LED (λ_{exc} = 405 nm) (no H_2O_2 added).

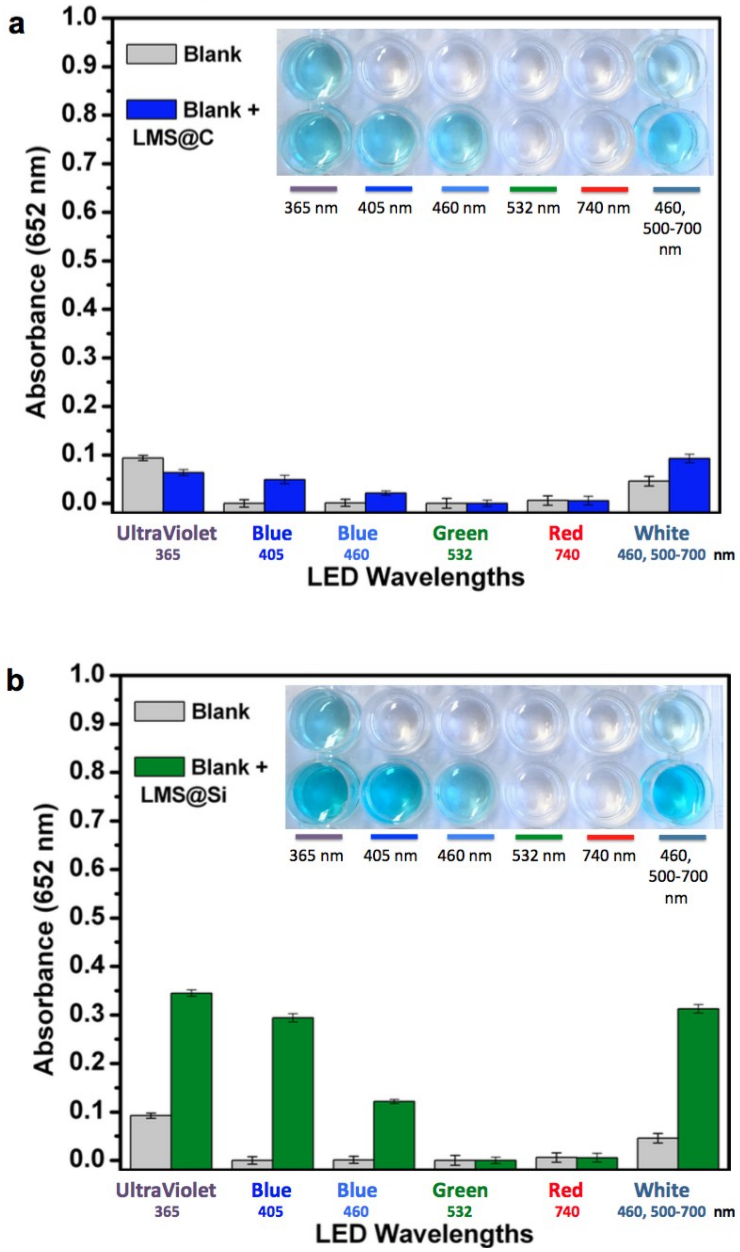

Fig. S8 Investigation of the effect of illuminating with different LED wavelengths on the photocatalytic activity of: a) LMS@C catalyst and b) LMS@Si catalyst. Experimental conditions: [catalyst] = 4 μg mL^{-1}; [TMB] = 0.16 mM; [H_2O_2] = 10 mM; pH = 7.4 (0.2 M NaAc buffer); total volume = 2mL; Irradiation time = 5 min (Inset: digital image of wells containing reaction mixtures after 5 min under irradiation with UV LED, blue LED-405, blue LED-460, green LED-532, red LED-740 and white LED, respectively). The error bars represent the standard deviation of three measurements.

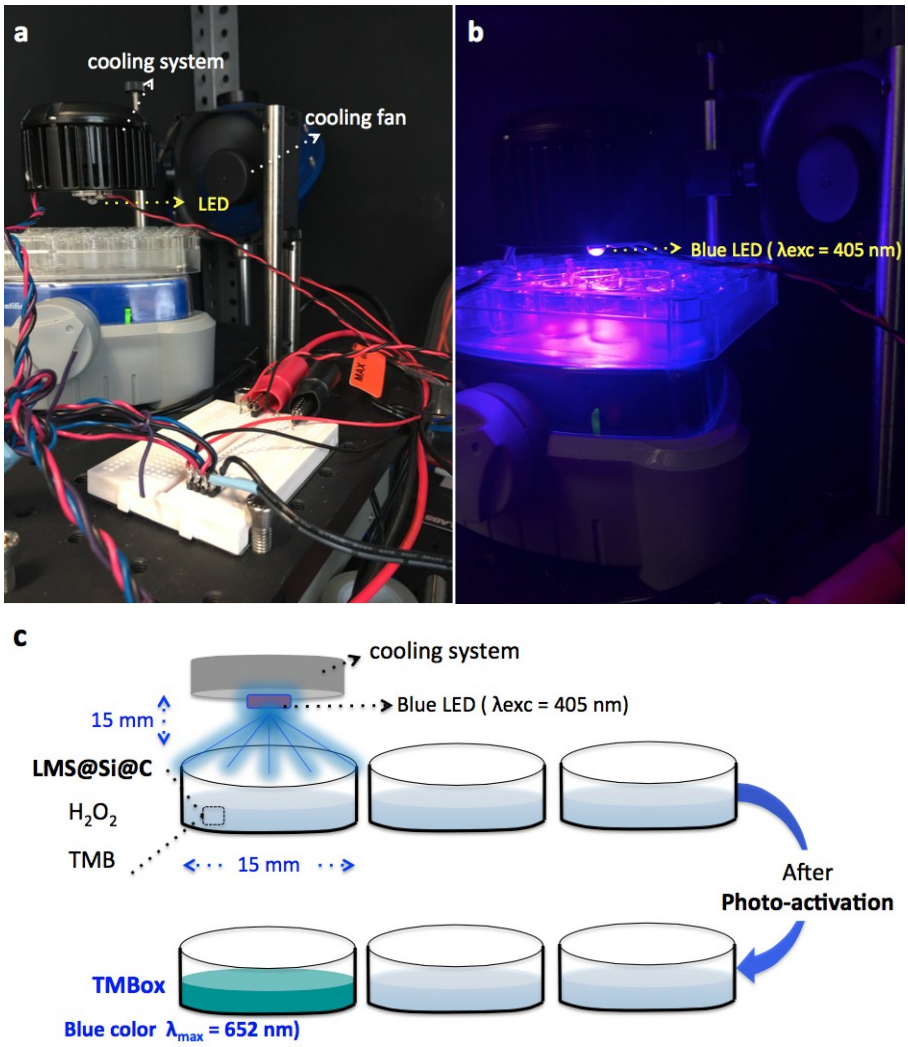

Figure S9. (a) Digital images of the experimental setup; (b) Digital image corresponding to the experimental setup while irradiating the cell culture wells with the blue-emitting LED (λ_{exc} = 405 nm); and (c) Schematic display of the experimental setup for peroxidase enzymatic assays using TMB performed in MW24 cell culture plates.

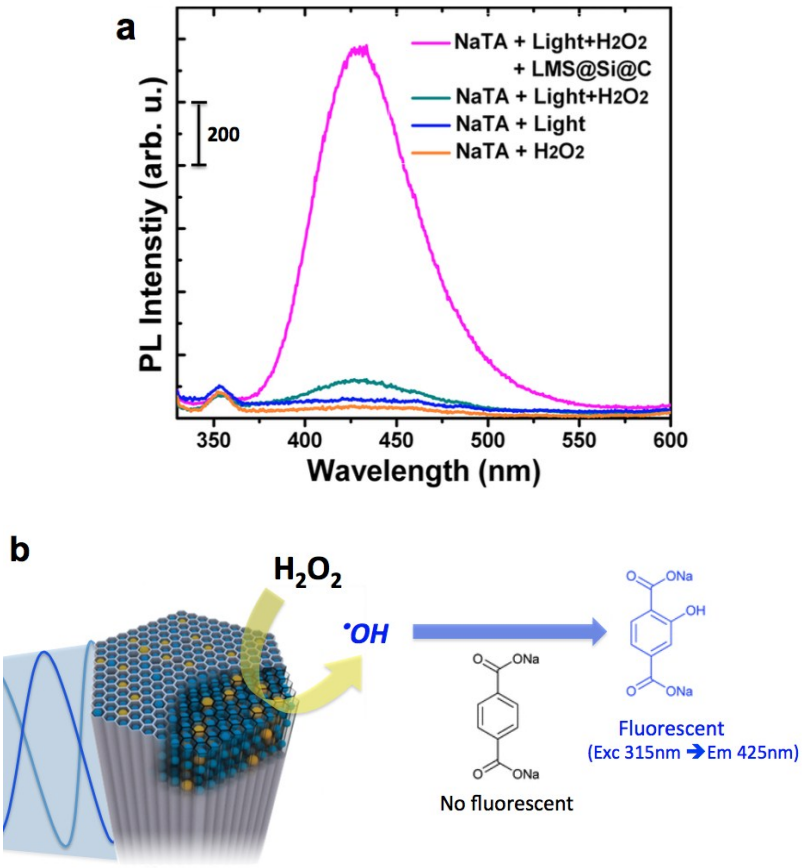

Fig. S10 a) Detection of hydroxyl radicals (•OH) generated from H_2O_2 using disodium terephthalate (NaTA) as a fluorescent probe emitting at 425 nm after reaction with the •OH radicals (fluorescence spectra taken from reaction aliquots at reaction time t = 5 min). Experimental details: $[H_2O_2]$ = 10 mM; [LMSs] = 4 µg mL^{-1}; [NaTA] = 5 mM; pH = 7.4 in 0.2 M NaAc buffer; irradiation experiments with a blue LED (λ_{exc} = 405 nm); and reaction temperature: 19-20 °C; specific dilutions and the generation of NaTA are further described in the experimental section; b) Schematic illustration of the colorimetric assay performed to identify the presence of hydroxyl radicals using disodium terephthalate (NaTA): The reaction occurs between hydroxyl radicals generated *in situ* in the presence of the LMS catalysts under blue-LED irradiation and the NaTA molecule that forms a selectively hydroxylated fluorescent derivative.

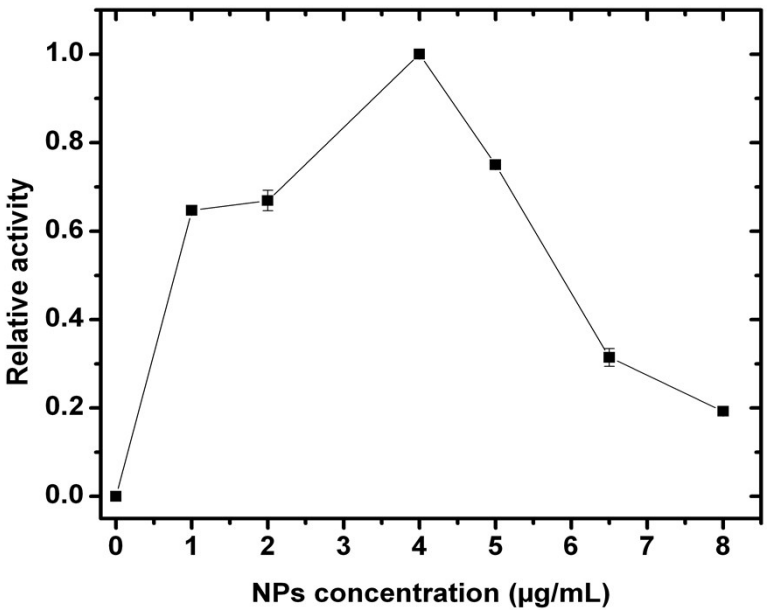

Fig. S11 Influence of the initial concentration of the LMS@Si@C sample on the performance as peroxidase-mimicking surrogate. Experimental details: [H_2O_2] = 10 mM; [LMSs] =different concentration, see graphic (0-1-2-4-5-6.5-8 μg mL^{-1}); [TMB] = 0.16 mM; pH = 7.4 in 0.2 M NaAc buffer; irradiation experiments with a blue LED (λ_{exc} = 405 nm); and reaction temperature: 19-20 °C.

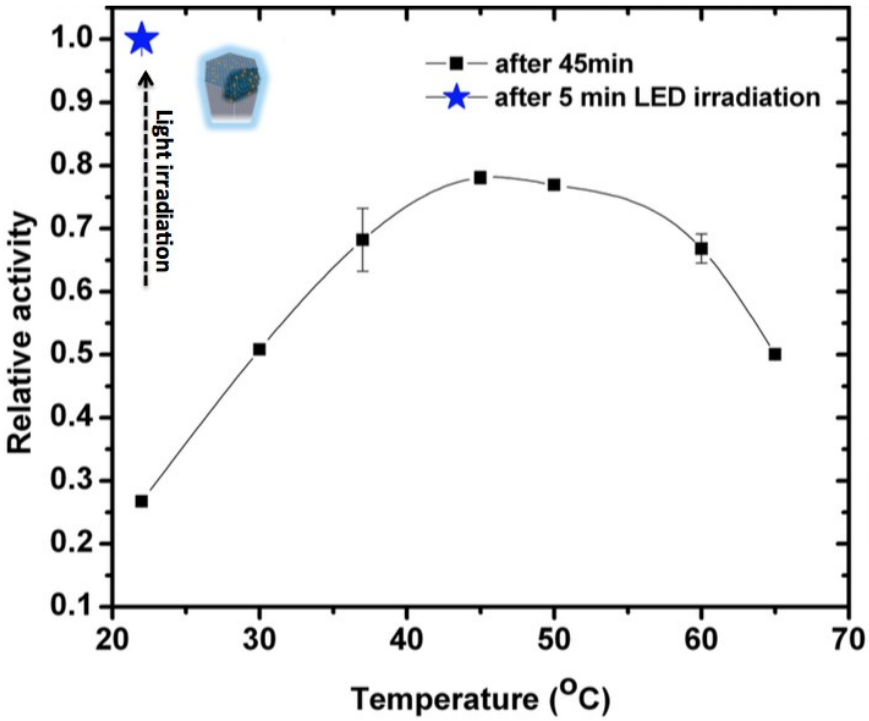

Fig. S12 Influence of the reaction temperature on the peroxidase-like activity of the LMS@Si@C catalyst (after 45 min reaction time). The response at room temperature following a 5 min illumination with a 405 nm LED light is also shown for comparison. Experimental details: $[H_2O_2]$ = 10 mM; [LMSs] = 4 μg mL^{-1}; [TMB] = 0.16 mM; pH = 7.4 in 0.2 M NaAc buffer; irradiation experiments with a blue LED (λ_{exc} = 405 nm) and reaction temperature: 19-20 °C; or without LED irradiation and different temperatures, 22-30-37-45-50-60-65 °C.

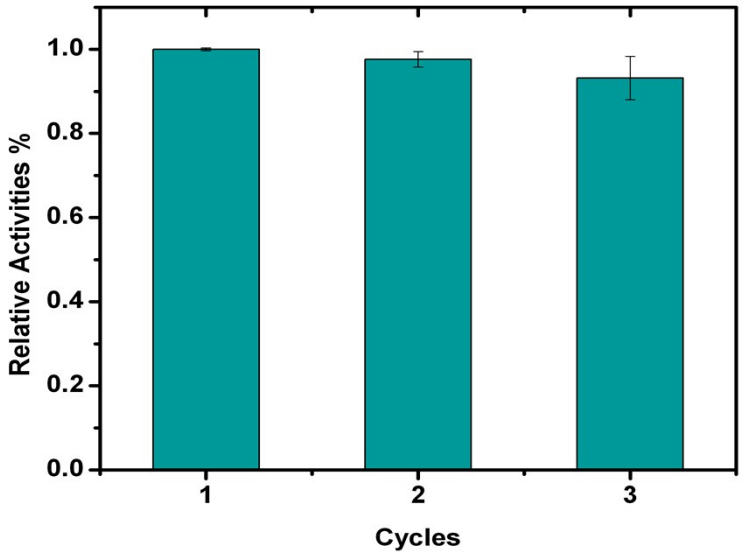

Fig. S13 Reusability of the peroxidase-like catalyst after 3 consecutive cycles.

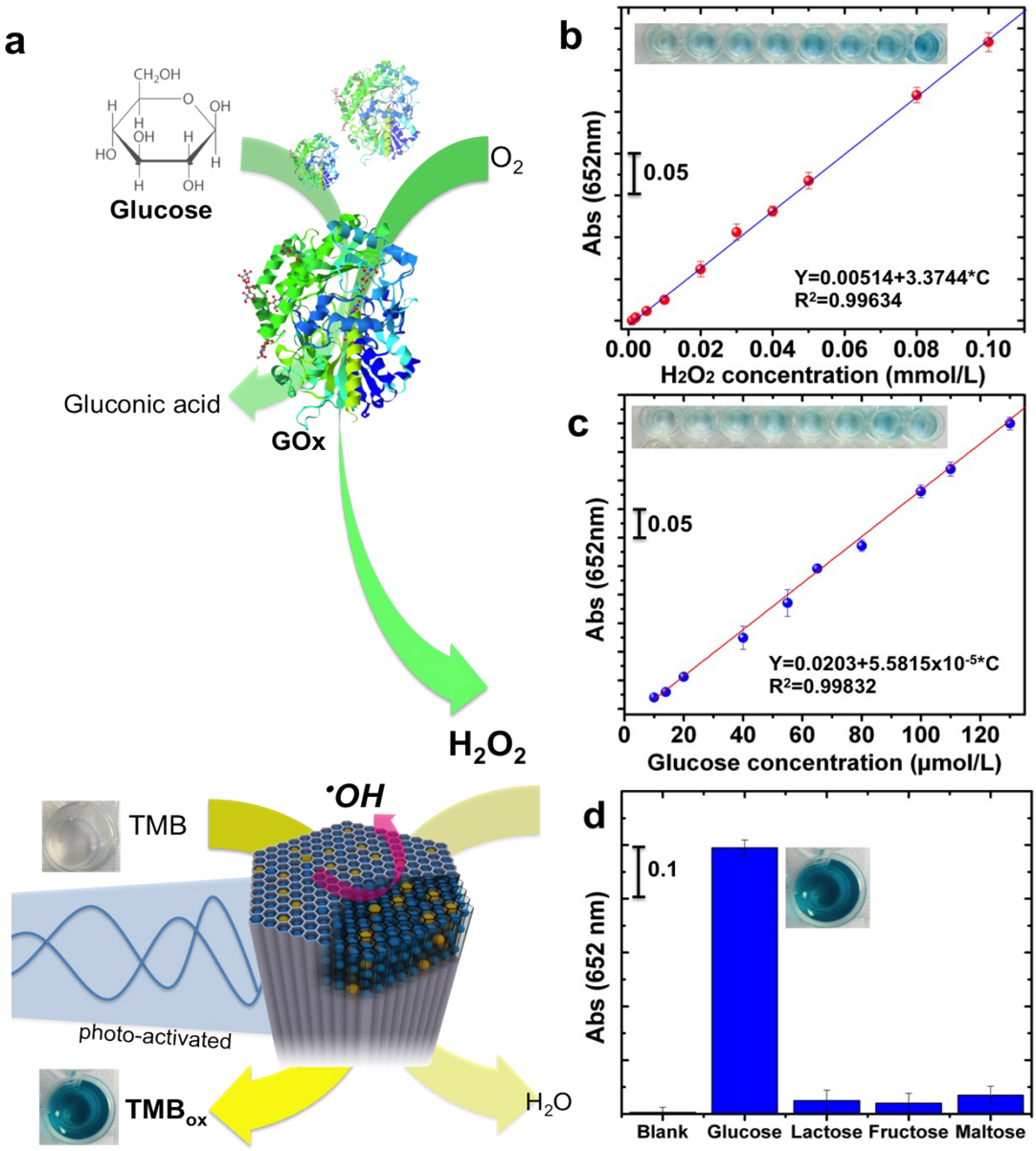

Figure S14. Use of the LMS@Si@C peroxidase-like photocatalyst in the indirect and selective detection of glucose: a) Schematic illustration of the cascade catalytic steps to indirectly detect glucose using the combination of a glucose oxidase natural enzyme and the peroxidase-like artificial mesoporous rod (LMS@Si@C). GOx oxidizes glucose to produce H_2O_2 that subsequently reacts with TMB in the presence of the peroxidase-like catalyst (LMS@Si@C); b) Evaluation of the lineal response to detect increasing concentrations of H_2O_2 concentration from 0.0010–0.10 mM with a detection limit (DL) of 1.5 μM; c) Evaluation of the indirect quantification of glucose (previously converted into gluconic acid and H_2O_2 by GOx) in the 10-130 μM range with a detection limit (DL) of 0.5 μM due to the selective reaction of the hydrogen peroxide in the presence of the catalyst; Error bars represent the standard deviation for three measurements; d) Determination of the selectivity of glucose detection with 10 mM lactose, 10 mM fructose, 10 mM maltose, and 10 mM glucose. The error bars represent the standard deviation of three measurements. Inset: The color change with the different solutions.

Electronic Supplementary Information References

1. W. Shi, Q. Wang, Y. Long, Z. Cheng, S. Chen, H. Zheng and Y. Huang, *Chemical Communications*, 2011, **47**, 6695-6697.
2. Q. Chen, M. Liu, J. Zhao, X. Peng, X. Chen, N. Mi, B. Yin, H. Li, Y. Zhang and S. Yao, *Chemical Communications*, 2014, **50**, 6771-6774.
3. Y. Z. Wang, W. J. Qi and Y. J. Song, *Chemical Communications*, 2016, **52**, 7994-7997.
4. Y. J. Song, Y. Chen, L. Y. Feng, J. S. Ren and X. G. Qu, *Chemical Communications*, 2011, **47**, 4436-4438.
5. L. N. Song, C. Huang, W. Zhang, M. Ma, Z. W. Chen, N. Gu and Y. Zhang, *Colloids and Surfaces a-Physicochemical and Engineering Aspects*, 2016, **506**, 747-755.
6. Y. J. Song, K. G. Qu, C. Zhao, J. S. Ren and X. G. Qu, *Advanced Materials*, 2010, **22**, 2206-2210.
7. Y. Tao, Y. H. Lin, Z. Z. Huang, J. S. Ren and X. G. Qu, *Advanced Materials*, 2013, **25**, 2594-2599.
8. Y. F. Zhang, C. L. Xu and B. X. Li, *Rsc Advances*, 2013, **3**, 6044-6050.
9. Y. L. Dong, H. G. Zhang, Z. U. Rahman, L. Su, X. J. Chen, J. Hu and X. G. Chen, *Nanoscale*, 2012, **4**, 3969-3976.
10. Q. An, C. Y. Sun, D. Li, K. Xu, J. Guo and C. C. Wang, *Acs Applied Materials & Interfaces*, 2013, **5**, 13248-13257.
11. J. Qian, X. W. Yang, L. Jiang, C. D. Zhu, H. P. Mao and K. Wang, *Sensors and Actuators B-Chemical*, 2014, **201**, 160-166.
12. M. C. Kim, D. Lee, S. H. Jeong, S. Y. Lee and E. Kang, *Acs Applied Materials & Interfaces*, 2016, **8**, 34317-34326.
13. S. Liu, J. Q. Tian, L. Wang, Y. L. Luo and X. P. Sun, *Rsc Advances*, 2012, **2**, 411-413.
14. G. Darabdhara, B. Sharma, M. R. Das, R. Boukherroub and S. Szunerits, *Sensors and Actuators B-Chemical*, 2017, **238**, 842-851.
15. K. F. Li, C. F. Chen, C. Y. Chen, Y. Z. Wang, Z. Wei, W. D. Pan and T. Song, *Enzyme and Microbial Technology*, 2015, **72**, 72-78.
16. J. Peng and J. Weng, *Biosensors & Bioelectronics*, 2017, **89**, 652-658.
17. H. W. Huang, L. F. Liu, L. Y. Zhang, Q. Zhao, Y. Zhou, S. S. Yuan, Z. L. Tang and X. Y. Liu, *Analytical Chemistry*, 2017, **89**, 666-672.
18. G. L. Wang, L. Y. Jin, Y. M. Dong, X. M. Wu and Z. J. Li, *Biosensors & Bioelectronics*, 2015, **64**, 523-529.
19. T. R. Lin, L. S. Zhong, J. Wang, L. Q. Guo, H. Y. Wu, Q. Q. Guo, F. F. Fu and G. N. Chen, *Biosensors & Bioelectronics*, 2014, **59**, 89-93.
20. G. L. Wang, X. F. Xu, L. Qiu, Y. M. Dong, Z. J. Li and C. Zhang, *Acs Applied Materials & Interfaces*, 2014, **6**, 6434-6442.
21. S. K. Maji, A. K. Dutta, S. Dutta, D. N. Srivastava, P. Paul, A. Mondal and B. Adhikary, *Applied Catalysis B-Environmental*, 2012, **126**, 265-274.
22. S. K. Maji, A. K. Dutta, D. N. Srivastava, P. Paul, A. Mondal and B. Adhikary, *Journal of Molecular Catalysis a-Chemical*, 2012, **358**, 1-9.
23. H. W. Wang, W. W. Jiang, Y. W. Wang, X. L. Liu, J. L. Yao, L. Yuan, Z. Q. Wu, D. Li, B. Song and H. Chen, *Langmuir*, 2013, **29**, 3-7.